An artificial vector model for generating abnormal electrocardiographic rhythms

Gari D Clifford[1,2,3]**, Shamim Nemati**[2,3] **and Reza Sameni**[4]

[1] Institute of Biomedical Engineering, Department of Engineering Science, University of Oxford, UK
[2] Massachusetts Institute of Technology, Cambridge, MA, USA
[3] Div. of Sleep Medicine, Dept. of Medicine, Harvard University, Boston, MA, USA
[4] School of Electrical and Computer Engineering, Shiraz University, Shiraz, Iran

E-mail: gari@robots.ox.ac.uk, shamim@mit.edu and rsameni@shirazu.ac.ir

Abstract

We present generalizations of our previously published artificial models for generating multi-channel ECG to provide simulations of abnormal cardiac rhythms. Using a three-dimensional vectorcardiogram (VCG) formulation, we generate the normal cardiac dipole for a patient using a sum of Gaussian kernels, fitted to real VCG recordings. Abnormal beats are specified either as perturbations to the normal dipole or as new dipole trajectories. Switching between normal and abnormal beat types is achieved using a first-order Markov chain. Probability transitions can be learned from real data or modeled by coupling to heart rate and sympathovagal balance. Natural morphology changes from beat-to-beat are incorporated by varying the angular frequency of the dipole as a function of the inter-beat (RR) interval. The RR interval time series is generated using our previously described model whereby time- and frequency-domain heart rate (HR) and heart rate variability characteristics can be specified. QT-HR hysteresis is simulated by coupling the Gaussian kernels associated with the T-wave in the model with a nonlinear factor related to the local HR (determined from the last n RR intervals). Morphology changes due to respiration are simulated by introducing a rotation matrix couple to the respiratory frequency. We demonstrate an example of the use of this model by simulating HR-dependent T-wave alternans (TWA) with and without phase-switching due to ectopy. Application of our model also reveals previously unreported effects of common TWA estimation methods.

Keywords: electrocardiogram, ECG modeling, hidden Markov models, TWA, T-wave alternans

(Some figures in this article are in colour only in the electronic version)

1. Introduction

This paper presents an extension of our previously described multi-lead electrocardiogram (ECG) model (McSharry *et al* 2003, Clifford *et al* 2005, Clifford 2006, Sameni *et al* 2007) to simulate the morphological dynamics of abnormal electrocardiographic rhythms. The motivation for this model was to provide a set of standard signals for the ninth annual PhysioNet-Computers in Cardiology Challenge (PCinCC) 2008 (Moody 2008), which aims to improve the understanding of methods for identification and analysis of ECG T-wave alternans (TWA). However, the general framework presented here is applicable to modeling the dynamics and morphology of any set of beats or rhythm.

Macro-level TWA, first reported by Hering (1908), is defined as the beat-to-beat oscillation of the amplitude of the T-wave that generally repeats every other beat. Microvolt TWA, first reported by Adam *et al* (1981), is widely understood to be an important indicator of risk of sudden cardiac death (Albrecht *et al* 1996). Although a variety of algorithms for TWA quantification have been proposed, testing the limits of these algorithms in the context of signal processing is difficult, since humans cannot score microvolt fluctuations, and it is unclear whether normal subjects exhibit TWA (Kaufman *et al* 2000). Therefore, assembling a population of test subjects is not possible. Moreover, testing TWA algorithms for varying levels of noise and artifacts can be difficult, requiring clean data that have already been scored. The existence of an accurate model for simulating the phenomenology of TWA therefore permits an objective assessment of the flaws and strengths of such algorithms.

2. Methods

2.1. Dynamic VCG model

Following McSharry *et al* (2003), Clifford *et al* (2005), Clifford (2006), Sameni *et al* (2007), and using a single dipole approximation for the cardiac potentials (Malmivuo and Plonsey 1995), the dynamics of the cardiac dipole vector $\mathbf{d}(t) = x(t)\hat{\mathbf{a}}_x + y(t)\hat{\mathbf{a}}_y + z(t)\hat{\mathbf{a}}_z$ can be modeled as

$$\dot{\theta} = \omega$$

$$\dot{x} = -\sum_i \frac{\alpha_i^x \omega}{(b_i^x)^2} \Delta\theta_i^x \exp\left[-\frac{(\Delta\theta_i^x)^2}{2(b_i^x)^2}\right]$$

$$\dot{y} = -\sum_i \frac{\alpha_i^y \omega}{(b_i^y)^2} \Delta\theta_i^y \exp\left[-\frac{(\Delta\theta_i^y)^2}{2(b_i^y)^2}\right] \tag{1}$$

$$\dot{z} = -\sum_i \frac{\alpha_i^z \omega}{(b_i^z)^2} \Delta\theta_i^z \exp\left[-\frac{(\Delta\theta_i^z)^2}{2(b_i^z)^2}\right],$$

where $\theta \in [-\pi, \pi]$ is the *cardiac phase* (Sameni *et al* 2007), $\Delta\theta_i^x = (\theta - \theta_i^x) \bmod (2\pi)$, $\Delta\theta_i^y = (\theta - \theta_i^y) \bmod (2\pi)$, $\Delta\theta_i^z = (\theta - \theta_i^z) \bmod (2\pi)$, $\omega = 2\pi h/(60\sqrt[\varsigma]{h_{av}})$, where h is the instantaneous (beat-to-beat) heart rate in beats per minute (BPM), h_{av} is the mean of the last n heart rates (typically with $n = 6$) normalized by 60 BPM and $\sqrt[\varsigma]{h_{av}}$ accounts for Bazett or Fredericia-like corrections for $\varsigma = 2$ and 3, respectively (Hodges 1997).

The first equation in equations (1) generates a circular trajectory rotating with the frequency of the heart rate. Each of the three coordinates of the dipole vector $\mathbf{d}(t)$ is modeled by a summation of Gaussian functions with amplitudes α_i^x, α_i^y and α_i^z; widths b_i^x, b_i^y and b_i^z; and located at rotational angles θ_i^x, θ_i^y and θ_i^z. Equations (1) can also be considered as a

model for generating orthogonal lead vectorcardiogram (VCG) signals (Sameni *et al* 2007). Moreover, the center of the Gaussian functions $\left(\theta_i^x, \theta_i^y \text{ and } \theta_i^z\right)$ are selected such that the R-peak is concentrated around $\theta = 0$. Therefore, the cardiac phase θ, which linearly sweeps the $[-\pi, \pi]$ range in each ECG beat, makes its transition from π to $-\pi$ after the T-wave and before the P-wave, i.e., in the *isoelectric* segment of the ECG. This transition point is later used for switching between the different beat types.

The multi-channel ECG is then generated by

$$\mathbf{ECG}(t) = H \cdot R \cdot \Lambda \cdot \mathbf{s}(t) + \mathbf{w}(t), \tag{2}$$

where $\mathbf{ECG}(t) \in \mathbb{R}^N$ is a vector of the ECG channels recorded from N leads, $\mathbf{s}(t) = [x(t), y(t), z(t)]^T \in \mathbb{R}^3$ contains the three components of the dipole vector $\mathbf{d}(t)$, $H \in \mathbb{R}^{N \times 3}$ corresponds to the body volume conductor model (or the inverse Dower transformation matrix (Dower *et al* 1980)), $\Lambda = \text{diag}(\lambda_x, \lambda_y, \lambda_z) \in \mathbb{R}^{3 \times 3}$ is a diagonal matrix corresponding to the scaling of the dipole in each of the x, y and z directions, $R \in \mathbb{R}^{3 \times 3}$ is the rotation matrix for the dipole vector, and $\mathbf{w}(t) \in \mathbb{R}^N$ is the noise in each of the N ECG channels at the time instant t. Note that H, R and Λ matrices are generally functions of time.

2.2. Generating the RR time series

The base RR interval time series $h_b(t)$ is generated as per McSharry *et al* (2003), with a baseline heart rate of 110 BPM, a standard deviation of 5 BPM and an LF/HF-ratio of 2 (see McSharry *et al* (2003)). However, any reasonable variants of these parameters can be chosen.

For the PCinCC 2008 (Clifford and Sameni 2008), we used $h_r(t) = \rho \tanh[\kappa (t - t_0)] + \upsilon$, where the parameters ρ, κ, t_0 and υ are arbitrary variables that control the shape and location of the ramp and by selecting these parameters as random variables, a randomly-seeded heart rate (HR) time series was generated. For later simulations, we adopt $\rho = 10$ BPM, $\kappa = 0.1\,\text{s}^{-1}$, $t_0 = 140$ s and $\upsilon = 0$. No ectopy, respiration or heart rate turbulence (HRT) dynamics were present in the data.

2.3. VCG generation: normal and abnormal beats

The dipole model in equations (1) is very generic and by using sufficient numbers of Gaussian functions, it can be used for synthesizing, both, normal and abnormal beats. Depending on the type of abnormality, abnormal beats can either have a totally different morphology, as compared to normal beats, or may have minor differences in specific parts. For example, in some of our simulations for generating realistic TWA time series, the normal beats were modeled with 11 Gaussian functions and abnormal beats (every second beat in the TWA time series) were generated by adding an offset to the 11th Gaussian amplitude (α_{11}). Alternatively, for the data in the PCinCC 2008, the α_i in equations (1), were modified to $\lambda \alpha_i$ for $i = 9, 10$ and 11. The diagonal matrix Λ is generally a three-dimensional quantity corresponding to each of the three VCG planes (Vx, Vy and Vz). To mimic the observation by Martínez and Olmos (2005) that there is a preferred plane of TWA activity, we arbitrarily forced the scaling to be different in each plane ($\lambda_x = 2\lambda_y = 3\lambda_z$). Twelve different levels of TWA activity were then generated (1 $\mu V \leqslant$ TWA amplitude $\leqslant 40\,\mu$V).

Figure 1 illustrates an example of the resultant VCG with a sampling frequency of 500 Hz. Figure 2 illustrates the 'ABAB' phenomenon of the resulting TWA effect with an offset amplitude of 23 μV, and figure 3 illustrates the effect of the T-wave alternation from beat to beat.
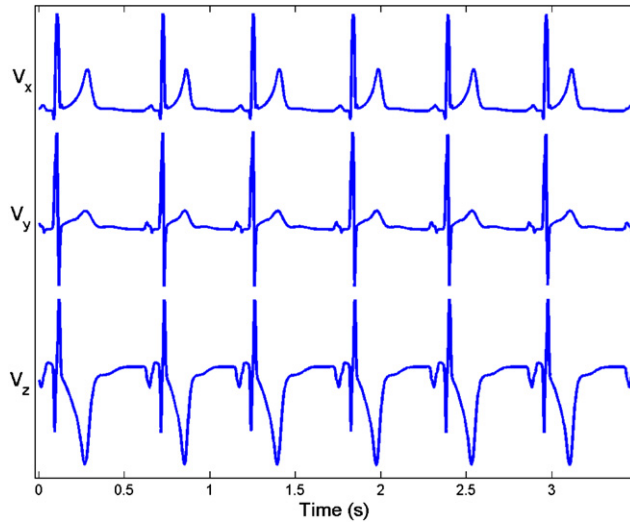
Figure 1. Example of VCG generated by the model from equations (1).
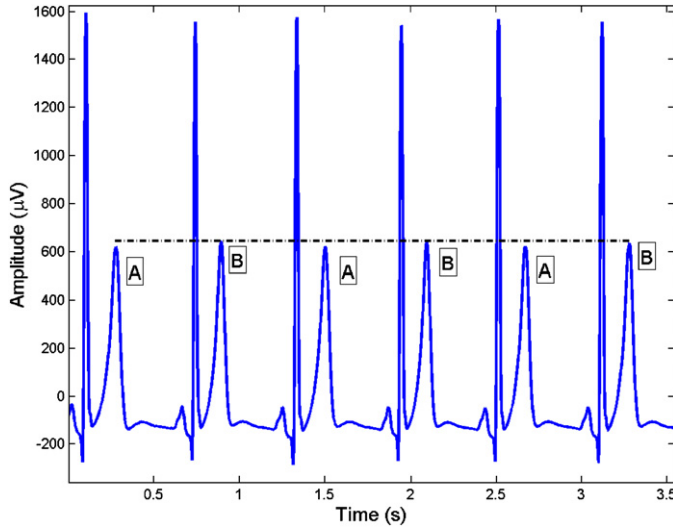
Figure 2. Typical alternating 'ABAB' TWA pattern (with TWA amplitude of 23 μV) generated from our model.

2.4. State transition matrix for TWA HR dependence

The transition from one beat type to another can be modeled within a probabilistic framework using a first-order Markov chain[5]. Considering each beat (normal or abnormal) as a state, the

---

[5] The assumption of a first-order Markov chain is only to simplify the training of the model parameters from relatively short data sets. Generalization to higher-order Markov chains is straightforward.
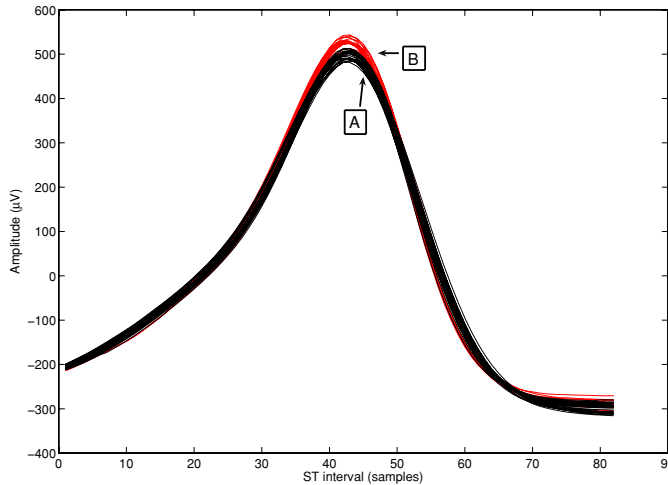
Figure 3. Multiple ST-T segments from two beat classes taken from one of the VCG projections. Class A beats are black and class B beats are grey.
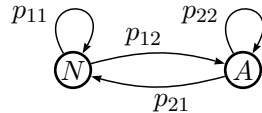
Figure 4. State transition graph between normal (N) and abnormal (A) beats using a first-order Markov chain. The graph can be extended to more abnormal beat types.

state transition matrix (STM) is defined as follows:

$$\text{STM} = \begin{bmatrix} p_{11} & p_{12} \\ p_{21} & p_{22} \end{bmatrix} \tag{3}$$

where, as shown in figure 4, the p_{ij} ($0 \leqslant p_{ij} \leqslant 1$) are the transition probabilities from normal (N) to abnormal (A) beats and vice versa. For the TWA application we chose a symmetric formulation, $\text{STM} = [1 - p \; p; \; p \; 1 - p]$, so that the probability of transition of normal to abnormal beats is the same as the probability of transition from abnormal to normal. (Also, to follow the convention of TWA, the two beat types are denoted A and B, although both are strictly abnormal.) In general this may not be true, since for some patients, the prevalence of ectopic beats may be biased toward runs of ectopy, rather than isolated ectopic beats. For TWA we have two extremes: *stationary continuous TWA* and *normal sinus rhythms*, which are achieved by setting $p = 1$ and $p = 0$, respectively. Of course, the STM has the same rank as the number of beat types and a similar probabilistic framework may be used for generating more than two beat types (see figure 5). Equation (3) then takes on the dimension of the number of beat types.

It is known that cardiac abnormalities such as the TWA are more probable in higher heart rates (Narayan 2006). Therefore, to simulate the dependence on HR of the TWA effect, we modify p to

$$p(t) = (\tanh[\vartheta(h(t) - h_{\text{TWA}})] + 1)/2, \tag{4}$$
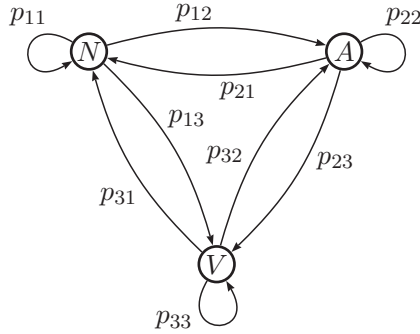
Figure 5. State transition graph between normal (*A*), abnormal (*B*) and ectopic (*V*) beats using a first-order Markov chain.
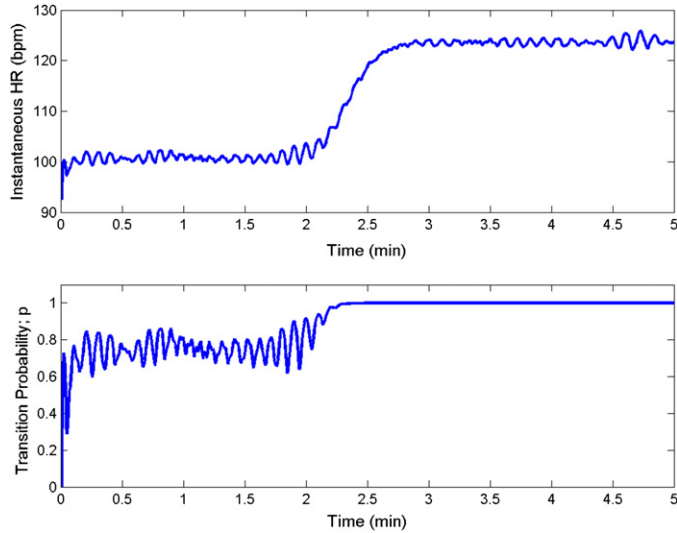
Figure 6. Example of instantaneous heart rate and resultant probability of transition to TWA.

where $h(t)$ is the instantaneous heart rate defined in equation (6), $h_{\text{TWA}} = 95 \pm 5$ BPM is the typical HR range at which the TWA effect manifests, and $\vartheta = 0.2$ BPM^{-1} controls the typical slope of transition. Furthermore, we require $0 \leqslant p(t) \leqslant 1$ to satisfy the requirements of a probability function.

Figure 6 illustrates an example of instantaneous heart rate and the resultant probability of transition to TWA derived from such a procedure. Note that as the instantaneous heart rate rises above 110 BPM, the transition probability saturates to unity (corresponding to continuous stationary TWA).

The STM is used to generate random states for switching between different beat types. Following the VCG model presented in section 2.1, to generate synthetic ECG, the state transition (or the choice of beat type) is made at the point of phase wrapping, where the cardiac phase θ jumps from π to $-\pi$.
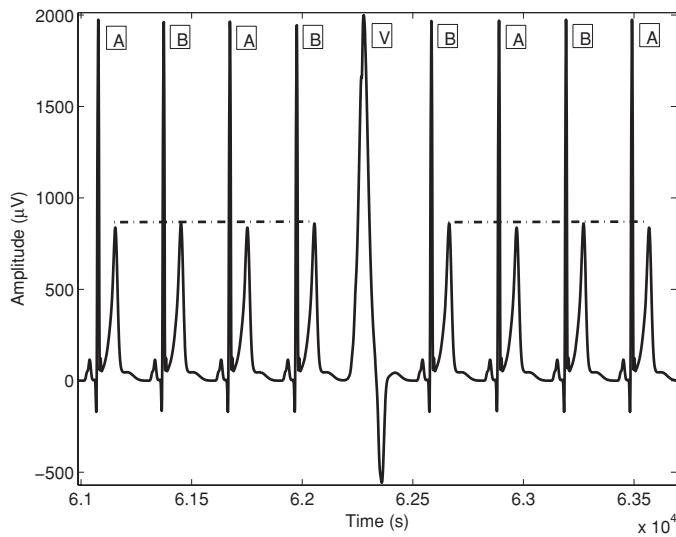
Figure 7. 'ABAB' beat sequence followed by a phase-changing ectopic beat (*V*). Note that the beats following the ectopic beat will now be of a 'BABA pattern'.

2.5. Modeling the effect of ectopy

To add ectopic beats into the model, three steps are necessary. First, a new morphological representation of the dipole is required (by fitting Gaussians in the three VCG dimensions to a known ectopic beat recorded in a VCG). Second, the ectopic beat must be placed earlier in the RR interval sequence. In the case of a premature ventricular beat, this is achieved by shortening the RR interval by between 10% and 30% (Clifford *et al* 2002) (and lengthening the following RR interval by a corresponding amount). The exact amount by which the two RR intervals are modified is determined by sampling from a uniform distribution. Third, the STM must become a three-by-three to represent the probabilities of transition from an A-type beat to a B-type, from an A-type to a V-type (ectopic beat) and from a B-type to a V-type beat, and vice versa. The probability of no change in beat type must also be programmed into the sequence (see figure 5). The STM effectively dictates whether there will be a TWA phase transition after an ectopic beat. For example, if P(B|V) is much greater than P(A|V), when P(V|B) is much higher than P(V|A), then as an ectopic beat occurs, a phase transition is likely[6]. That is, we see an 'ABABVBABA' sequence rather than an 'ABABVABAB' sequence. Similarly, if the P(A|V) is much greater than P(B|V), when P(V|A) is much higher than P(V|B), then a symmetrical phase transition is likely. That is, we see a 'BABAVABAB' sequence rather than a 'BABAVBABAB' sequence.

   Figure 7 illustrates the effect of an ectopic beat in the 'ABAB' beat sequence, whereby a phase change results and the following beats exhibit a 'BABA' pattern.

2.6. Adding the effect of respiration

Recall from equation (2) that the no-noise ECG can be represented from the product $H \cdot R \cdot \Lambda \cdot \mathbf{s}(t)$. Although the product $H \cdot R \cdot \Lambda$ may be assumed to be a single matrix,

---

[6] P(X|Y) denotes the probability of transition from *X* to *Y*.

the representation in equation (2) has the benefit that the rather stationary features of the body volume conductor that depend on the location of the ECG electrodes and the conductivity of the body tissues can be considered in H, while the temporal inter-beat movements of the heart can be considered in Λ and R, meaning that their average values are identity matrices in a long-term study: $E\{R\} = I$ and $E\{\Lambda\} = I$.

However, on a short-term timescale (a few seconds), Λ and R represent the translation and rotation of the heart with respect to the sensors as the subject breathes in and out. R can therefore be modified by the Givens rotations (Sameni *et al* 2007), with a time-varying angle, ϕ as described by Astrom *et al* (2000).

The angular variation around each axis is modeled by the product of two sigmoidal functions reflecting inhalation and exhalation, such that for lead X the rotation angle (in degrees) is defined at the nth sample index as

$$\phi_X(n) = \sum_{p=0}^{\infty} \zeta_X \frac{1}{1 + e^{-\varrho_i(p)(n - \kappa_i(p))}} \frac{1}{1 + e^{-\varrho_e(p)(n - \kappa_e(p))}}, \qquad (5)$$

where

$$\varrho_i(q) = 20 \frac{f_r(q)}{f_s}, \qquad \kappa_i(q) = \kappa_i(q - 1) + \frac{f_s}{f_r(q - 1)}, \qquad \kappa_i(0) = 0.35 f_s,$$

$$\varrho_e(q) = 15 \frac{f_r(q)}{f_s}, \qquad \kappa_e(q) = \kappa_e(q - 1) + \frac{f_s}{f_r(q - 1)}, \qquad \kappa_e(0) = 0.6 f_s,$$

q denotes each respiratory cycle index, $1/\varrho_i(q)$ and $1/\varrho_e(q)$ are the duration of inhalation and exhalation, respectively, $\kappa_i(q)$ and $\kappa_e(q)$ are the time delays of the sigmoidal functions, f_s is the sampling rate, $f_r(q)$ is the respiratory frequency and ζ_X is the maximum angular variation around lead X, which has been set to $5°$. The same procedure is applied to leads Y and Z, with $\zeta_Y = \zeta_Z = \zeta_X$.

The VCG, V, is therefore transformed on a sample-by-sample basis with the three-dimensional rotation matrix $R(\phi)$ which leads to realistic amplitude variations in each axis that manifest as the familiar QRS area or RS amplitude variation (Baílon *et al* 2006). The entire VCG is then generated using equation (2). Figure 9 illustrates the effect of adding respiration in this manner.

Note that for the simulated data in the PCinCC 2008, we set $\Lambda = I$, in order to contain all movement with respect to the sensors in the R matrix. Note also that the inverse Dower matrix, H, is not square and therefore generates a more numerous set of leads than the existing VCG as described in the next section.

2.7. Generation of full 12-lead ECG

To generate five different *artificial patients*, we used the model parameters in Sameni *et al* (2007) and derived a set of five individual Dower transforms (IDTs) (Dower *et al* 1980) using the first five patients in the Physikalisch-Technische Bundesanstalt Diagnostic ECG Database (PTBDB) (Bousseljot *et al* 1995, Kreiseler and Bousseljot 1995). We denote these matrices by H_j, where $j = 1, 2, \ldots, 5$. The PTBDB consists of 549 records from 290 subjects with 15 simultaneously measured signals: the conventional 12 leads (I, II, III, AVR, AVL, AVF, V1, V2, V3, V4, V5, V6) together with the 3 Frank lead ECGs (Vx, Vy, Vz). The individual (3 by 12) Dower matrix is derived from a nonlinear least square optimization fit (Marquardt 1963) between the VCG and the 12 ECG leads, using the first 10 s of each patient. Although such a method ignores the changes in the IDT from beat to beat due to respiration, morphological changes due to respiration are already accounted for in the model, using a
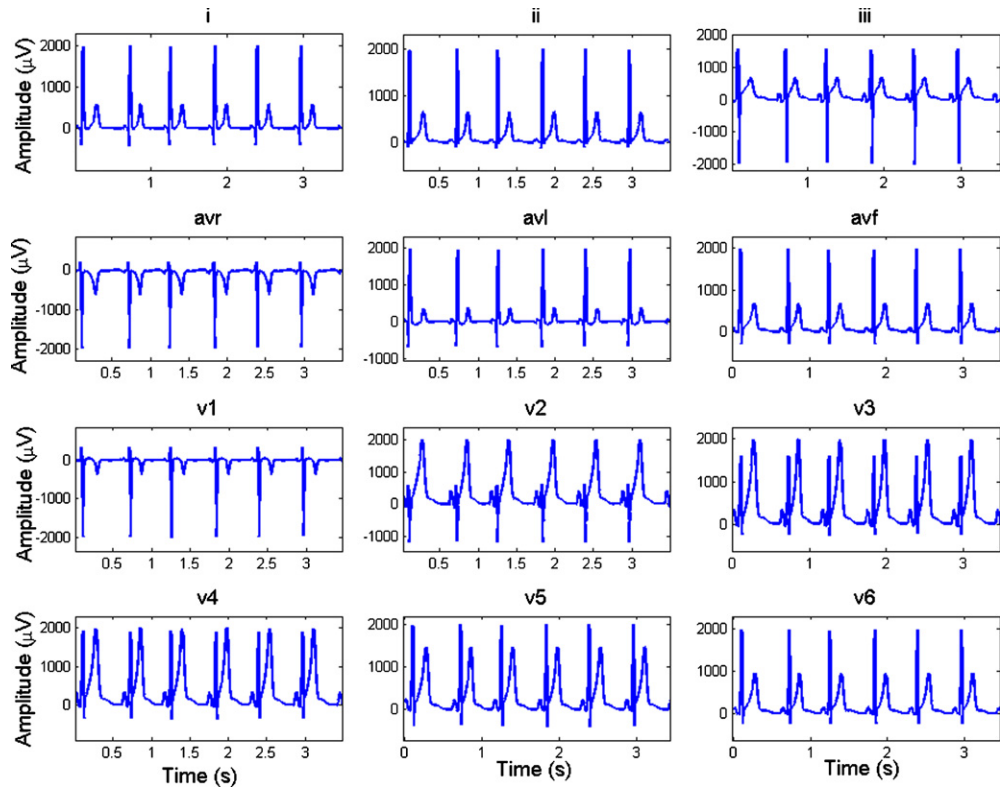
Figure 8. Example of 12 lead ECG after application of IDT.
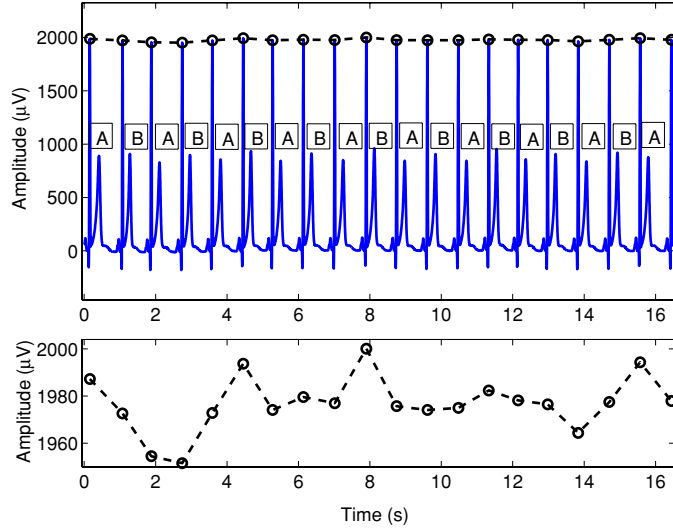
Figure 9. Example of the x-axis of a generated VCG ($f_s = 500$ Hz) with added respiratory effect (upper plot). A low frequency modulation of the R-peaks at the respiratory frequency ($f_r = 16$ breaths min^{-1}) is evident (lower plot). Note that the TWA effect (48 μV) is also modified by the respiration so that the ABAB sequence is no longer uniform.
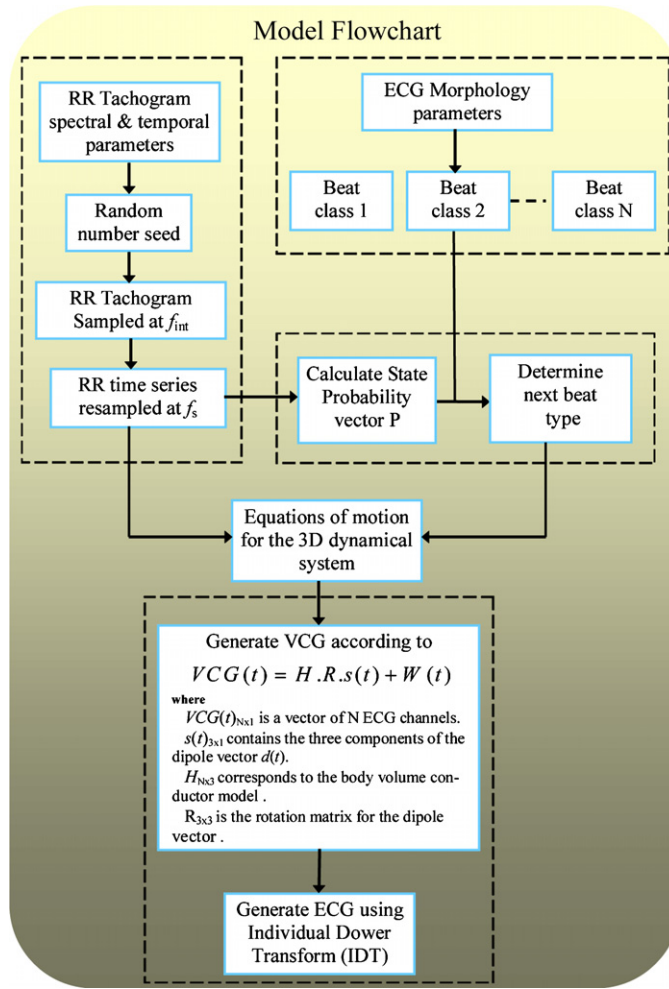
Figure 10. Logical flow of processes required to generate the abnormal rhythm model.

Bazett-like correction (McSharry *et al* 2003) to the Gaussian parameters. Application of each IDT to the VCG, together with randomized seeds for the RR interval generation, provides 12-lead ECG for the five different patients.

The complete logical flow of the process required to generate the abnormal rhythm model is given in figure 10. Note that the RR generation procedure, beat morphology modeling, state probability transmission and multi-lead generation (through the IDT) are all separate processes that can be replaced by any other reasonable model. In particular, the RR interval time series generation can be altered to mimic any particular activity or event.

2.8. Generic biophysical modeling

As we described in Clifford and McSharry (2004) and Clifford (2006), the model presented here is quite general for replicating quasi-periodic activity, particularly for biomedical applications. The transition probabilities can be learned from recorded data of an individual or a population. Furthermore, the model may be extended to incorporate other models of RR interval variation,
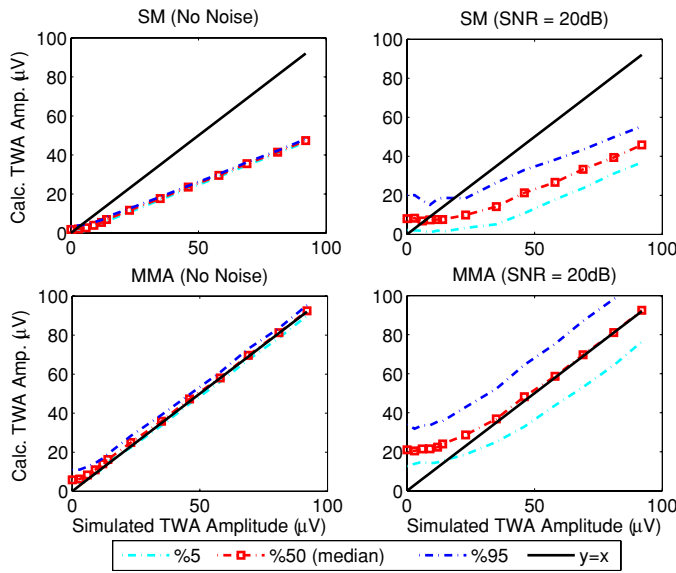
Figure 11. Performance of SM (upper) and MMA method (lower) for TWA estimation with no noise or respiration (left) and 20 dB realistic noise (right).

and extended to other quasi-periodic signals. One obvious extension to this model is that of blood pressure, where inter-beat variations in pulse morphology can follow a Markov chain-like variation.

3. Results

In order to evaluate our simulator we used visual inspection to empirically verify the TWA amplitudes with no QT variation. In tests we generated TWA amplitudes of 2, 3, 4, 5, 6, 7, 8, 10, 11, 12, 20, 30 and 40 μV for each of the five artificial patients, with the rotation matrix, R, set to be the identity matrix.

The generated 12-lead ECG for one of the realizations of this model is illustrated in figure 8 and the corresponding VCG from which this 12-lead example is derived (using the IDT) is illustrated in figure 1.

The overall logic flow for generating our multi-lead ECG model with abnormal and normal beats is illustrated in figure 10. Using the winner of the open-source division of the PCinCC 2008 (Khaustov *et al* 2008), we found that our model faithfully reproduced TWA activity at all input levels. This is as expected, since the model mathematically guarantees this effect.

However, when we examined the performance of traditional TWA estimators, such as the modified moving average (MMA) (Verrier and Nearing 1994, Nearing and Verrier 2002) and the spectral method (SM) (Adam *et al* 1981, Albrecht *et al* 1996) (also using open source algorithms from the PCinCC 2008 (Khaustov *et al* 2008)), we found discrepancies at both low and high TWA levels. Figure 11 (left) illustrates the performance of the SM (upper plot) and MMA method (lower plot) in estimating TWA from our simulator. Note that the SM consistently underestimates the actual value of the TWA amplitude. Note also that the MMA

method produces a false TWA amplitude of 5 μV $\pm$ 5 μV TWA when there is actually no TWA present.

Moreover, when noise was added, either as independent background noise or as physiological variability (due to respiratory influence for example, with $R \neq I$), the TWA activity can be seen to cause false-negative and false-positive detections in some detectors, because some natural T-wave morphology variation exists, particularly over the respiratory cycle. Figure 11 (right) illustrates the effect of the SM (upper plot) and MMA method (lower plot) at 20 dB background noise. (The noise was taken from the Noise Stress Test Database on PhysioNet (Goldberger *et al* 2000).) Note that the noise floor (at 0 μV) has risen, causing false triggering in both estimation methods.

4. Model limitations and future work

Besides the baseline rhythms, the RR interval can also be influenced by sudden increases or decreases, long-term variations in the order of minute or higher, and state-dependent phenomena such as *heart rate turbulence* (Bauer *et al* 2006) (a rapid acceleration and deceleration after an ectopic beat (Bauer *et al* 2006)). These effects have not been explicitly added to the model, but can simply be achieved by adding additional terms to the base RR interval time series:

$$h(t) = h_b(t) + h_r(t) + h_{\mathrm{HRT}}(t) + \cdots, \tag{6}$$

where $h_r(t)$ is a function that models the long-term variations of the RR interval, $h_{\mathrm{HRT}}(t)$ models the HRT phenomenon and $h(t)$ is the resulting time-varying RR interval time series, which forms the input for ω in equations (1).

HRT after an ectopic beat is characterized by an increase of HR followed by a decrease back to the baseline rate (Bauer *et al* 2006). Therefore, we selected $h_{\mathrm{HRT}}(t) = h_0(t) * f_{\mathrm{imp}}(t)$, where $h_0(t)$ is the difference of two log-normal shapes to model the HRT, $*$ represents the convolution operator and $f_{\mathrm{imp}}(t)$ is an impulse function that is fired whenever we reach an ectopic (V-type) beat.

However, we do not model the sympathetic and parasympathetic changes that occur during HRT. In fact, dynamic CNS coupling to our model is not modeled at all. Since a HR increase is likely to be due to either a parasympathetic withdrawal, or sympathetic innervation, or a combination of both, we should couple the LF-HF ratio to HR in a nonlinear manner. Although this would be fairly simple in the context of our model, picking the correct relationship is not trivial. A likely approach would be to introduce a model such as that of DeBoer (deBoer *et al* 1987), to allow the coupling of HR and heart rate variability (HRV), though this does not address the need to couple the effects of HR, HRV and arrhythmias.

Evidence does exist that the sympathetic nervous system is capable of a direct arrhythmogenic influence on the ischemic myocardium independent of the heart rate (Euler *et al* 1985), although an exact mathematical relationship has not been defined. The existence of TWA in patients with congenitally long QT syndrome, which can be exacerbated or provoked by excitement or emotional or physical stress, suggests that sympathetic stimulation may be important to the mechanism of TWA (Schwartz and Malliani 1975, Verrier *et al* 1992, Euler *et al* 1996, Estes *et al* 1997, Hohnloser *et al* 1997). However, since the effect is still controversial, and some authors have demonstrated that TWA is mostly a HR-related effect (Kaufman *et al* 2000), we have not included any explicit coupling of the TWA activity with the sympathetic nervous system in our model.

Moreover, by employing a HMM, it is possible to learn the exact dynamics from a given patient, or a population, and avoid the question of having to build an exact model of these

relationships. In fact, if we know that HR is a large influence on the transition matrix, we may explicitly add HR into the state vector and learn the state transition matrix with the HR-dependence included. Give the above observations of HRT, it is likely that the rate of change of HR should also be included in the state, so that a given beat, at a given ω and $\Delta\omega/\Delta t$, has a transition probability to another beat type, ω and $\Delta\omega/\Delta t$. Of course, modifications are required to quote with a HMM that has a mixed state space consisting of continuous and discrete parts.

We also note that variations in TWA amplitudes are introduced by changing the value of Λ in equation (2). Although this appears to be a time-independent vector which scales the dipole, Λ could be a time-varying parameter that is coupled to the heart rate, for example, which increases in magnitude at higher heart rates. Gradual changes could also be coupled to specific interventions such as balloon inflations. This would reflect the observations by Martínez *et al* (2006) that TWA amplitudes vary gradually over time.

5. Discussion and conclusions

The dynamic model presented in this paper is fully generalizable, using an optimization procedure to fit the VCG to any given subject or observation to an arbitrary level of accuracy. The rotating dipole vector model presented here is rather general, since the *universal approximation* property of Gaussian mixtures means that any continuous function (as the dipole vector is assumed to be so) can be modeled with a sufficient number of Gaussian functions up to an arbitrarily close approximation (Ben-Arie and Rao 1995). Each beat class can be fitted to real examples separately, and the probability transition matrix that determines how likely it is for one beat type to follow another can be derived from empirical studies of known databases. The STM is coupled to heart rate, but can also be coupled to autonomic tone, sleep state or any other relevant input parameter. Therefore, abnormal beats such as ectopy can be simulated by using new beat classes (fitted in the same manner as the derivation of the IDT), and adding an appropriate shortening of the associated RR interval. Each new beat class increases the rank of the STM by one. An appropriate transition probability between this new beat and other beat classes can be derived by training the HMM on real databases.

Since our model employs a dipole representation, with a Dower-like transform to map the dipole back onto clinical observational axes (such as the standard 12-lead ECG), correlated noise can be added in multiple dimensions, and hence can manifest in a realistic manner on all observational ECG leads. Multiple noise sources can be treated as other dipole moments in the model, and the relative motions of sources and sensors can be simulated using a Givens rotation matrix to multiply the IDT (Sameni *et al* 2007). Finally, clinical features of the simulated signal can be extracted directly from the model (Clifford 2006, Clifford and Villarroel 2006) to provide a gold standard for evaluating signal processing algorithms.

As an illustration of the application of the model presented in this paper, we evaluated two standard TWA metrics. Results demonstrate that intrinsic systematic errors exist in both metrics. In particular, for small TWA amplitudes ($\leqslant 10\ \mu$V), both methods overestimate or falsely trigger, even at extremely low (or no) noise level. This effect may partly explain observations that 'natural' TWA activity of normal subjects of up to 10 μV has been reported in healthy subjects (Kaufman *et al* 2000). Note also that the noise floor at which TWA activity is falsely recorded rises as the background noise rises. Therefore, during periods of elevated noise (such as during exercise, when the HR is elevated and TWA are reported as more common), we expect to see more false episodes of TWA, and an overestimation of the overall magnitude of the effect. Such issues should be factored into the clinical employment of these algorithms, and adjustments made accordingly. For example, it is common to employ

statistical methods to reject TWA activity that may have been generated by noise alone. However, such techniques generally assume stationary noise, and pick quiescent periods in which the 'no-TWA' baseline noise level can be determined. Our simulations indicate that this is likely to lead an overestimation of the magnitude of the TWA activity at low levels.

Acknowledgments

References

Adam D R, Akselrod S and Cohen R J 1981 Estimation of ventricular vulnerability to fibrillation through T-wave time series analysis *Comput. Cardiol.* **8** 307–10

Albrecht P, Arnold J, Krishnamachari S and Cohen R J 1996 Exercise recordings for the detection of T-wave alternans: promises and pitfalls *J. Electrocardiol.* **29** Suppl 46–51

Astrom M, Santos E, Sornmo L, Laguna P and Wohlfart B 2000 Vectorcardiographic loop alignment and the measurement of morphologic beat-to-beat variability in noisy signals *IEEE Trans. Biomed. Eng.* **47** 497–506

Baílon R, Sornmo L and Laguna P 2006 A robust method for ECG-based estimation of the respiratory frequency during stress testing *IEEE Trans. Biomed. Eng.* **53** 1273–85

Bauer A, Malik M, Barthel P, Schneider R, Watanabe M A, Camm A J, Schömig A and Schmidt G 2006 Turbulence dynamics: an independent predictor of late mortality after acute myocardial infarction *Int. J. Cardiol.* **107** 42–7

Ben-Arie J and Rao K 1995 Nonorthogonal representation of signals by Gaussians and Gabor functions *IEEE Trans. Circuits Syst.* **42** 402–13

Bousseljot R, Kreiseler D and Schnabel A 1995 Nutzung der EKG-Signaldatenbank CARDIODAT der PTB uber das Internet *Biomed. Tech.* **40** S317–8

Clifford G D 2006 A novel framework for signal representation and source separation *J. Biol. Syst.* **14** 169–83

Clifford G D and McSharry P E 2004 Generating 24-hour ECG, BP and respiratory signals with realistic linear and nonlinear clinical characteristics using a nonlinear model *Comput. Cardiol.* **31** 709–12

Clifford G D, McSharry P E and Tarassenko L 2002 Characterizing abnormal beats in the normal human 24-hour RR tachogram to aid identification and artificial replication of circadian variations in human beat to beat heart rate *Comput. Cardiol.* **29** 129–32

Clifford G D and Sameni R 2008 An artificial multi-channel model for generating abnormal electrocardiographic rhythms *Comput. Cardiol.* **35** 773–6

Clifford G D, Shoeb A, McSharry P E and Janz B A 2005 Model-based filtering, compression and classification of the ECG *Int. J. Bioelectromag.* **7** 158–61

Clifford G D and Villarroel M 2006 Model-based determination of QT intervals *Comput. Cardiol.* **33** 357–60

deBoer R W, Karemaker J M and Strackee J 1987 Hemodynamic fluctuations and baroreflex sensitivity in humans: a beat-to-beat model *Am. J. Physiol.* **253** H680–9

Dower G E, Machado H B and Osborne J A 1980 On deriving the electrocardiogram from vectorcardiographic leads *Clin. Cardiol.* **3** 87

Estes N A, Michaud G, Zipes D P, El-Sherif N, Venditti F J, Rosenbaum D S, Albrecht P, Wang P J and Cohen R J 1997 Electrical alternans during rest and exercise as predictors of vulnerability to ventricular arrhythmias *Am. J. Cardiol.* **80** 1314–8

Euler D E, Guo H and Olshansky B 1996 Sympathetic influences on electrical and mechanical alternans in the canine heart *Cardiovasc. Res.* **32** 854–60

Euler D E, Nattel S, Spear J F, Moore E N and Scanlon P J 1985 Effect of sympathetic tone on ventricular arrhythmias during circumflex coronary occlusion *Am. J. Physiol.* **249** H1045–50

Goldberger A L, Amaral L A N, Glass L, Hausdorff J M, Ivanov P C, Mark R G, Mietus J E, Moody G B, Peng C-K and Stanley H E 2000 PhysioBank, PhysioToolkit, and PhysioNet: components of a new research resource for complex physiologic signals *Circulation* **101** e215–20

Hering H E 1908 Das wesen des herzalternans *Münchener. Med. Wochenschr.* **4** 1417–21

Hodges M 1997 Rate correction of the QT interval *Cardiac. Electrophysiol. Rev.* **3** 360–3

Hohnloser S H, Klingenheben T, Zabel M, Li Y G, Albrecht P and Cohen R J 1997 T wave alternans during exercise and atrial pacing in humans *J. Cardiovasc. Electrophysiol.* **8** 987–93

Kaufman E S, Mackall J A, Julka B, Drabek C and Rosenbaum D S 2000 Influence of heart rate and sympathetic stimulation on arrhythmogenic T wave alternans *Am. J. Physiol. Heart Circ. Physiol.* **279** H1248–55

Khaustov A, Nemati S and Clifford G D 2008 An open-source standard T-wave alternans detector for benchmarking *Comput. Cardiol.* **35** 509–12

Kreiseler D and Bousseljot R 1995 Automatisierte EKG-Auswertung mit hilfe der EKG-Signaldatenbank CARDIODAT der PTB *Biomed. Tech.* **40** S319–20

Malmivuo J A and Plonsey R (ed) 1995 *Bioelectromagnetism, Principles and Applications of Bioelectric and Biomagnetic Fields* (Oxford: Oxford University Press)

Marquardt D W 1963 An algorithm for least-squares estimation of nonlinear parameters *SIAM J. Appl. Math.* **11** 431–41

Martínez J P and Olmos S 2005 Methodological principles of T wave alternans analysis: a unified framework *IEEE Trans. Biomed. Eng.* **52** 599–613

Martínez J P, Olmos S, Wagner G and Laguna P 2006 Characterization of repolarization alternans during ischemia: time-course and spatial analysis *IEEE Trans. Biomed. Eng.* **53** 701–11

McSharry P E, Clifford L, Tarassenko G D and Smith L 2003 A dynamical model for generating synthetic electrocardiogram signals *IEEE Trans. Biomed. Eng.* **50** 289–94

Moody G B 2008 The Physionet / Computers in Cardiology Challenge 2008: T-wave alternans *Comput. Cardiol.* **35** 505–8

Narayan S M 2006 *Ch 7: Pathophysiology Guided T-Wave Alternans Measurement (Engineering in Medicine and Biology vol 1)* 1st edn (Norwood, MA: Artech House) pp 196–214

Nearing B D and Verrier R L 2002 Modified moving average analysis of T-wave alternans to predict ventricular fibrillation with high accuracy *J. Appl. Physiol.* **92** 541–9

Sameni R, Clifford G D, Shamsollahi M B and Jutten C 2007 Multi-channel ECG and noise modeling: application to maternal and fetal ECG signals *EURASIP J. Adv. Signal Processing* **2007** 1–14

Schwartz P J and Malliani A 1975 Electrical alternation of the T-wave: clinical and experimental evidence of its relationship with the sympathetic nervous system and with the long q-t syndrome *Am. Heart. J.* **89** 45–50

Verrier R L, Dickerson L W and Nearing B D 1992 Behavioral states and sudden cardiac death *Pacing Clin. Electrophysiol.* **15** 1387–93

Verrier R L and Nearing B D 1994 Electrophysiologic basis for t wave alternans as an index of vulnerability to ventricular fibrillation *J. Cardiovasc. Electrophysiol.* **5** 445–61